6. Lamb DJ, Bullock DW, Hoyte RM, et al. Δ^9-[16α-^{125}I]iodo-19-nortestosterone: a gamma-emitting photoaffinity label for the progesterone receptor. *Endocrinology* 1986;122:1923–1932.
7. Ali H, Rousseau J, Van Lier JE. Synthesis of (17α,20E/Z) iodovinyl testosterone and 19-nortestosterone derivatives as potential radioligands for androgen and progesterone receptors. *J Steroid Biochem Mol Biol* 1994;49:15–29.
8. Liu A, Dence CS, Welch MJ, et al. Fluorine-18-labeled androgens: radiochemical synthesis and tissue distribution studies on six fluorine-substituted androgens, potential imaging agents for prostatic cancer. *J Nucl Med* 1992;33:724–734.
9. Hoyte RM, Rosner W, Hochberg RB. Synthesis of [16α-^{125}I]iodo-5α-dihydrotestosterone and evaluation of its affinity for the androgen receptor. *J Ster Biochem* 1982;16:621–628.
10. Hoyte RM, MacLusky NJ, Hochberg RB. The synthesis and testing of E-17α-(2-iodovinyl)-5α-dihydrotestosterone and Z-17α-(2-iodovinyl)-5α-dihydrotestosterone as γ-emitting ligands for the androgen receptor. *J Ster Biochem* 1990;36:125–132.
11. Hochberg RB, Rosner W. The interaction of 16α-[^{125}I]iodoestradiol with estrogen receptor and other binding proteins. *Proc Natl Acad Sci USA* 1980;77:328–332.
12. Hanson RN, Franke LA. Preparation and evaluation of 17α-[^{125}I]iodovinyl-11β methoxyestradiol as a highly selective radioligand for tissues containing estrogen receptors. *J Nucl Med* 1984;25:998–1002.
13. Hoyte RM, Brown TJ, MacLusky NJ, et al. 7α-Methyl-17α-(E-2′-[^{125}I]iodovinyl)-19-nortestosterone: a new radioligand for the detection of androgen receptor. *Steroids* 1993;58:13–23.
14. Hoyte RM, Borderson K, Bryson K, et al. Synthesis and evaluation of 7α-Iodo-5α-dihydrotestosterone as a potential radioligand for androgen receptor. *J Med Chem* 1994;37:1224–1230.
15. Olah GA, Hussain A, Singh BP, et al. Synthetic methods and reactions, 112. Synthetic transformations with trichloromethylsilane/sodium iodide reagent. *Am Chem Soc* 1983;83:3667–3672.
16. Zava DT, Landrum B, Horwitz KB, et al. Androgen receptor assay with [^{3}H] methyltrienolone (R1881) in the presence of progesterone receptors. *Endocrinology* 1979;104:1007–1012.
17. Ginsberg M, Greenstein BD, MacLusky NJ, et al. An improved method for the study of high affinity steroid binding: oestradiol binding in brain and pituitary. *Steroids* 1974;23:773–792.
18. Munson PJ, Rodbard D. LIGAND. A versatile computerized approach for characterization of ligand-binding systems. *Anal Biochem* 1980;107:220–239.
19. Delean A, Munson PJ, Rodbard D. Simultaneous analysis of families of sigmoidal curves: application to bioassay, radioligand assay, and physiological dose-response curves. *Am J Physiol* 1978;235:E97–E102.
20. Brown TJ, Sharma M, MacLusky NJ. Localization and measurement of occupied androgen receptors in thaw-mounted rat and human prostate tissue sections by in vitro autoradiography. *Steroids* 1995;60:239–243.
21. Kumar V, Amann A, Ourisson G, et al. Stereospecific syntheses of 7β- and 7α-hydroxycholesterols. *Syn Commun* 1987;17:1279–1286.
22. Cragg GML, Davey CW, Hall DN, et al. Hydroxy-steroids, part IV. The preparation and spectra of steroid olefins. *J Chem Soc* 1966:1266–1276.
23. Cremlyn RJW, Shoppe CW. Steroids and walden inversion, part XVI. The epimeric cholestan-7-ols. *J Chem Soc* 1954:3515–3518.
24. Horwitz KB, Costlow ME, McGuire WL. MCF-7: a human breast cancer cell line with estrogen, androgen, progesterone and glucocorticoid receptors. *Steroids* 1975:785–795.
25. Dube JY, Chapdelaine P, Tremblay RR, et al. Comparative binding specificity of methyltrienolone in human and rat prostate. *Hormone Res* 1995;7:341–347.
26. Corvol P, Bardin CW. Species distribution of testosterone-binding globulin. *Biol Reprod* 1973;8:277–282.
27. Kreig M. Characterization of the androgen receptor in the skeletal muscle of the rat. *Steroids* 1976;28:261–274.
28. Still CW, Kahn M, Mitra A. Rapid chomatographic technique for preparative separations with moderate resolution. *J Org Chem* 1978;43:2923–2925.

Variables Influencing Tumor Dosimetry in Radioimmunotherapy of CEA-Expressing Cancers with Anti-CEA and Antimucin Monoclonal Antibodies

Thomas M. Behr, Robert M. Sharkey, Malik E. Juweid, Robert M. Dunn, Zhiliang Ying, Cun-H. Zhang, Jeffry A. Siegel and David M. Goldenberg

Garden State Cancer Center at the Center for Molecular Medicine and Immunology, Newark; Department of Statistics, Rutgers University, Piscataway; and Department of Radiation Oncology, Cooper Hospital/University Medical Center, Camden, New Jersey

In this study, we examined the factors that may influence tumor dosimetry in the radioimmunotherapy of solid, CEA-expressing cancers. **Methods:** Data from 119 tumors in 93 patients with CEA-expressing cancers were analyzed. The patients underwent radioimmunotherapy with the ^{131}I-labeled IgG_1 anti-CEA antibodies NP-4 ($K_a = 10^8\ M^{-1}$) or MN-14 ($K_a = 10^9\ M^{-1}$), its humanized form hMN-14, as well as the anticolon-specific antigen-p (CSAp) antibody, Mu-9. For dosimetry, the biodistribution, targeting kinetics and cumulated activity of tumors and organs were determined from planar and SPECT imaging. **Results:** An inverse logarithmic relationship between tumor size and antibody uptake was found for both anti-CEA antibodies, whereas no such relationship was found for Mu-9. The absolute tumor uptake was identified as the most important factor determining the radiation dose to the tumor ($r = 0.9$), with the biological half-life of the antibody in the tumor being of secondary importance ($r = 0.5$). No significant difference in tumor uptake was found between both anti-CEA antibodies, despite their tenfold difference in affinity. At comparable masses, colorectal and medullary thyroid cancers had significantly higher tumor uptakes ($p = 0.02$), as well as tumor-to-red marrow dose ratios, than other cancer types. The tumor half-lives of the anti-CEA antibodies were significantly lower in colorectal than in all other tumor types ($p = 0.01$). **Conclusion:** In radioimmunotherapy, tumor uptake appears to be the most important dose-determining factor. Differences in antibody affinity are reflected by differences in the biological half-life, not the absolute uptake. Especially favorable conditions for anti-CEA antibodies seem to prevail in colorectal cancer patients having minimal disease, as well as in medullary thyroid cancer, where cytotoxic tumor doses might be expected. Antimucin antibodies may have a particular advantage in the treatment of patients with larger colorectal tumors.

Key Words: radioimmunotherapy; monoclonal antibodies; carcinoembryonic antigen; tumor dosimetry

J Nucl Med 1997; 38:409–418

Although radioimmunotherapy (RAIT) of lymphoma and other hematological tumors is increasingly being accepted as a potent new mode of treatment (*1,2*), its success in solid tumors is still limited (*2,3*). In preclinical models, RAIT of colorectal cancer has been shown to be more effective than an equitoxic chemotherapy of 5-fluorouracil and leucovorin (*4*). In an adjuvant (minimal metastatic disease) model, RAIT was shown to be highly effective for achieving even long-term cures (*5*). The biological, physiological, biophysical and biochemical conditions in such animal models, however, can be fundamentally different from the clinical situation (*6*). Mathematical

Received March 18, 1996; revision accepted June 15, 1996.

For correspondence or reprints contact: David M. Goldenberg, MD, Garden State Cancer Center, 520 Belleville Ave., Belleville, NJ 07109.

TABLE 1
Characteristics Patients with Solid, CEA-Expressing Tumors (n = 93)

Tumor type	MAb	No.	Plasma CEA range (ng/ml)	Blood $T_{1/2}$ (hr)	RM dose (cGy/mCi)	WB dose (cGy/mCi)
Colorectal cancer		59	2.8–6132			
	MN-14	21	2.8–6132			
Anti-CEA	hMN-14	9	295.2–2593	17.6 ± 12.6†	2.1 ± 1.0†	0.6 ± 0.3†
	NP-4	15	3.2–241			
Anti-CSAp	Mu-9	14	2.6–21644	41.7 ± 12.4	3.8 ± 1.4	1.0 ± 0.2
Medullary thyroid cancer		9	3.6–373			
	MN-14	4	16.5–373			
Anti-CEA	hMN-14	3	9.5–27	40.0 ± 14.6	5.1 ± 1.2	1.0 ± 0.5
	NP-4	2	3.6–30			
Lung cancer		6	2.6–5.2			
Anti-CEA	MN-14	5	2.6–5.1	40.9 ± 9.4	4.0 ± 1.5	1.1 ± 0.4
	hMN-14	1	5.2			
Pancreatic cancer		3	3.6–79			
Anti-CEA	MN-14	2	2.6–79	36.0 ± 8.6	3.6 ± 1.5	1.0 ± 0.3
	NP-4	1	3.6			
Ovarian cancer		9	2.6–6.3			
Anti-CEA	MN-14	5	2.6–3.6	43.4 ± 20.8	4.8 ± 2.1	1.0 ± 0.4
	hMN-14	4	2.6–6.3			
Other cancer types		7	2.2–748			
Anti-CEA	MN-14	3	2.2–3.6			
	hMN14	2	5.1–748	55.5 ± 17.2	2.5 ± 0.6	0.7 ± 0.1
	NP-4	2	3.2–9.6			

*Since previous studies have shown identical pharmacokinetics of NP-4, MN-14, as well as its humanized form within the same tumor type (*12,19*), this table does not differentiate further between these MAbs.

†Blood half-lives, red marrow and whole-body doses are significantly lower ($p < 0.001$) with anti-CEA MAbs in colorectal cancer patients than in all other tumor types, or than with anti-CSAp in the same cancer type.

models (*7–9*) of parameters determining tumor targeting and uptake (e.g., tumor size, vascular permeability, interstitial pressure, as well as the presence of a binding site barrier) have been verified mostly by animal studies (*7–11*). Therefore, a closer examination of factors that influence tumor dosimetry in patients is warranted, since achieving sufficiently high tumor doses is paramount to accomplishing therapeutic efficacy in the RAIT of solid tumors (*2*). In a recent study, we analyzed in closer detail factors such as plasma tumor marker levels, antibody protein dose, the epitope recognized by the antibody and its affinity, which influence the kinetic and targeting behavior of anti-CEA and an antimucin antibody in patients with CEA-expressing tumors (*12*). Promising, but still limited therapeutic success, could be shown in a clinical trial with the ^{131}I-labeled anti-CEA monoclonal antibody, NP-4 (*13*) as well as its F(ab')$_2$ fragment (*14*), especially in patients with small lesions. An especially favorable dosimetry of anti-CEA antibodies was recently observed by Juweid et al. (*15*) in medullary thyroid cancer.

Therefore, the purpose of this study was to focus on factors that may influence the tumor dosimetry of solid, CEA-expressing tumors to identify those subgroups of patients where radioimmunotherapy may be promising. These findings could be used as a guideline in the design of future clinical trials.

MATERIALS AND METHODS

Antibodies and Radiolabeling

NP-4 and MN-14 are IgG$_1$-subclass murine anti-CEA monoclonal antibodies (*16,17*). Both are directed against the same class-III peptide epitope of the CEA molecule, according to the classification of Primus et al. (*18*); the affinity of MN-14 was determined to be tenfold higher than that of NP-4 (10^9 l/mole compared with 10^8 l/mole) (*12*). Recently, a humanized, CDR-grafted form of MN-14 was developed and introduced into clinical trials (*19*). The studies of Sharkey et al. showed identical biodistribution and tumor targeting properties of the humanized and murine forms of MN-14 (*19*).

Mu-9 is a murine monoclonal antibody of the IgG$_1$ subtype, directed against the colon-specific antigen-p mucin (CSAp), which is present in a high percentage of colorectal cancers (*20*). This antibody has the advantage of recognizing an epitope which is not present in the circulation.

The antibodies were purified by protein A and ion-exchange chromatography. Their final purity was tested by immunelectrophoresis, polyacrylamide gel electrophoresis using reducing and nonreducing conditions, and size-exclusion, high-pressure liquid chromatography (250 column, 300 × 7.8 mm) (*13,15,16*).

Radioiodination with Na^{131}I was performed by the chloramine-T or iodogen methods (*12*). The specific activity was 12–16 mCi/mg. Binding of the radioiodinated antibodies to a CEA-immunoadsorbent column was more than 80%. The immunoreactivity of labeled Mu-9 was tested by binding to an Affi-Gel-15 affinity column (Bio Rad, Richmond, CA) prepared by coupling of a mucin extract of the GW-39 human colon carcinoma cell line (*20*). Iodine-131-Mu-9 preparations had an immunoreactivity of 74.2% ± 7.5%.

CEA and HAMA Determinations

Plasma CEA levels were determined by using a CEA-EIA that was described earlier (*12*). The serum samples were heat-extracted before CEA measurement to avoid falsification of results by human antimouse antibodies (HAMA) present in patients' sera (*17,19*). HAMA titers were determined using a commercially available enzyme-linked immunoabsorbent assay. The normal range in this assay was less than 74 ng/ml. HAMA were determined immedi-

TABLE 2
Overall Tumor Dosimetry of Anti-CEA Mabs (NP-4, MN-14), Its Humanized Form and Anti-CSAp Mu-9 (HAMA- and HAHA-Negative Patients Only)

Antibody form	Tumor dose (cGy/mCi)	Tumor/Nontumor ratios					No.
		T/Red marrow	T/Whole body	T/Kidney	T/Liver	T/Lung	
MN-14 ^{131}I-IgG	9.7 ± 9.5	3.2 ± 2.5	12.4 ± 10.5	2.5 ± 2.7	3.4 ± 3.2	3.4 ± 2.2	59
hMN-14 ^{131}I-IgG	7.6 ± 5.7	2.7 ± 1.9	10.1 ± 7.6	1.7 ± 1.3	2.5 ± 2.0	2.8 ± 1.9	25
NP-4 ^{131}I-IgG	8.8 ± 3.2	3.4 ± 1.1	13.1 ± 4.1	2.8 ± 0.4	3.7 ± 1.3	3.7 ± 1.9	16
Mu-9 ^{131}I-IgG	14.9 ± 12.7	3.6 ± 2.5	14.1 ± 10.0	2.6 ± 2.6	3.8 ± 2.9	3.8 ± 3.0	19

ately before antibody administration, then in weekly intervals for the first 3 mo, and at least monthly in the following year.

Human antihumanized MN-14 (=anti-idiotypic) antibodies (called HAHA in this study, although they actually represent anti-idiotypic antibodies against the remaining murine portion of humanized MN-14) were determined by in vitro complexation studies, analyzed by HPLC (*19*). Briefly, 0.1 ml plasma, diluted 1:3 with acetate buffer, was added to 20 ng of ^{125}I-labeled hMN-14, incubated overnight at 4°C and analyzed by size-exclusion HPLC. The same analysis was done with a plasma sample that was heat-inactivated for 15 min in a 90°C water bath. The amount of complexed activity in the heat-extracted plasma was subtracted from the nonheat-extracted sample to give a final residual complexation. Any residual complexation >10% was considered as positive for HAHA.

Patient Selection

The data of 93 patients with CEA-expressing adenocarcinomas who underwent RAIT with the ^{131}I-labeled high-affinity IgG anti-CEA monoclonal antibody, MN-14 (n = 41), its humanized, CDR-grafted form hMN-14 (n = 19), the lower affinity anti-CEA IgG, NP-4 (n = 19) or the anti-CSAp antibody, Mu-9 (n = 14), were analyzed in this study (among them, 59 colorectal, 9 medullary thyroid, 6 lung, 3 pancreatic and 9 ovarian cancer patients; Table 1).

Antibody Administration

Before antibody injection, all patients were premedicated with Lugol's solution and potassium perchlorate to decrease the thyroid and gastric uptake, respectively (*12,17*). All patients entered into the RAIT protocol first underwent a diagnostic-dosimetric study with 0.5–2.5 mg of protein, labeled with 8.0–30.0 mCi ^{131}I, for assessment of tumor targeting and dosimetry. Usually within 2 wk after the dosimetric injection, the patients were admitted to the hospital for therapy (4.0–27.5 mg, 29.8–238.9 mCi).

Imaging

Scanning of patients was performed with a Sophy-DS-X or DS-7 camera (Sopha Medical Systems, Columbia, MD). Anterior and posterior planar images were obtained in diagnostic studies daily from 4 to 168 hr postinjection (occasionally up to 336 hr) with a high-energy parallel-hole collimator, collecting 500,000 counts on all days (128 × 128 matrix). In therapeutic settings (higher activities), imaging was started when the retained whole-body activity reached ≤30 mCi. SPECT was performed routinely at 24, 48, 72 and 96 hr (64 projections over 360°, 64 × 64 matrix size), using a Hamming-Hann filter for reconstruction.

Pharmacokinetic Analysis

MAb blood clearance rates were determined by counting blood samples at various times after the end of the infusion, as described previously (*12–17,19*). The clearance data are expressed as the biological clearance times as follows: half-life alpha ($t_{1/2}$-α: distribution phase); half-life beta ($t_{1/2}$-β: elimination phase); and (overall) half-life ($t_{1/2}$: number of hours required for 50% of the activity to be cleared from the blood, as calculated from bior monoexponential modeling, depending upon the best curve fit). Total-body clearance rates were determined from whole-body scans obtained from 4 hr postinjection until the end of imaging.

Dosimetry

ROIs of organs and tumors were generated from the anterior and posterior planar views obtained during each imaging session. Appropriate adjacent soft tissue regions served as background regions for the organs. The background regions for tumors were chosen in the normal, nontumor-bearing parenchyma of the respective organ, as close to the tumor as possible. The activities in these regions were generated by using the buildup factor methodology for Compton scatter compensation (*21*). The individual time-activity curves of organs and tumors were fit to a mono- or biexponential function by a nonlinear, least-squares analysis or by the trapezoidal method, and then integrated to obtain the cumulated activity in each region. The blood time-activity concentration data were also fit by a mono- or biexponential function to obtain the cumulated activity in the blood. The red marrow cumulated activity was calculated from these data by multiplying this concentration by 1500, as the assumed weight in grams of the marrow in an average adult. The mean dose in cGy was calculated for organs and tumors according to the Medical Internal Radiation Dose (MIRD) scheme, with correction for the remainder of the whole-body activity (*22–24*). For tumor dosimetry, the self-to-self, self-to-host, and host-to-self doses were considered. The masses of normal organs were generated from MIRD standard tables, and tumor volumes were obtained from CT or calculated by a voxel-counting procedure from SPECT data (*12*). If not otherwise stated, all data on tumor pharmacokinetics and dosimetry reported in this paper rely exclusively on studies where imaging was started no later than 48 hr after antibody administration (i.e., diagnostic or low-activity therapeutic injections), in order to avoid any bias of the results due to missing early phases of the tumor or organ kinetics (*12*). Reported maximum tumor uptake values were determined as the intercept of a pseudolinear back-extrapolation from the logarithm of measured uptake values with the ordinate ([i.e., the virtual uptake at the time of MAb injection (*22*)]).

Statistical Analysis

All reported values represent the arithmetic means with the corresponding s.d. Statistical analysis was performed by Student's t-test. Linear regression lines were fitted using the weighted least-squares method. Standard deviations were estimated via residuals, and pointwise 95% confidence intervals were constructed using normal distribution tables. Differences in the slopes of regression lines were assessed using a t-test constructed for this purpose. If there were several tumors in the same patient, the data of each tumor were considered separately. Whenever necessary, appropriate measures were taken to ensure the validity of the models used, including histogram plots and residual analysis. The data analysis and statistical computing were based on statistical software S (*25*).

TABLE 3
Tumor Dosimetry with Anti-CEA MN-14, NP-4 and Anti-CSAp Mu-9 According to Different Cancer Types

Antibody form	Tumor dose (cGy/mCi)	Tumor/Nontumor ratios					No.
		T/Red marrow	T/Whole body	T/Kidney	T/Liver	T/Lung	
Colorectal cancer							
MN-14	7.2 ± 6.2*	3.2 ± 2.2†	11.7 ± 9.8†	2.3 ± 2.2	3.3 ± 2.8	3.7 ± 2.1	33
hMN-14	6.7 ± 5.6*	3.5 ± 1.9†	12.0 ± 7.8†	1.6 ± 1.3	3.0 ± 2.2	3.5 ± 2.0	12
NP-4	6.3 ± 0.8*	2.9 ± 0.4†	10.7 ± 1.5†	N/D	2.8 ± 1.6	2.7 ± 0.4	10
Mu-9	14.9 ± 12.7*	3.6 ± 2.5†	14.1 ± 10.0†	2.6 ± 2.6	3.8 ± 2.9	3.8 ± 3.0	19
Medullary thyroid cancer							
MN-14	18.0 ± 10.7‡	5.0 ± 3.3†	18.2 ± 13.2†	3.7 ± 2.3	3.0 ± 1.4	3.9 ± 1.5	9
NP-4	11.3 ± 2.9‡	4.0 ± 1.4†	16.3 ± 4.3†	2.8 ± 0.4	4.8 ± 1.0	4.2 ± 2.7	4
Lung cancer							
MN-14	6.9 ± 3.2	1.9 ± 0.9	7.6 ± 3.0	1.1 ± 0.8	2.4 ± 1.4	1.6 ± 0.7	8
hMN-14	2.0	0.7	3.0	0.7	0.8	0.8	1
NP-4	N/D	N/D	N/D	N/D	N/D	N/D	—
Ovarian cancer							
MN-14§	8.9 ± 13.0	2.8 ± 3.6	12.9 ± 16.1	4.9 ± 6.2	5.2 ± 7.8	4.9 ± 6.3	8
hMN-14	6.8 ± 4.8	1.6 ± 1.0	5.8 ± 4.8	1.2 ± 0.6	1.9 ± 0.6	1.6 ± 1.2	5
NP-4	N/D	N/D	N/D	N/D	N/D	N/D	—
Pancreatic cancer							
MN-14	6.5 ± 5.2	1.3 ± 0.7	5.8 ± 4.2	2.4 ± 1.9	2.6 ± 2.5	1.9 ± 1.12	2
hMN-14	4.8	1.0	4.4	2.3	N/D	1.2	1
NP-4	N/D	N/D	N/D	N/D	N/D	N/D	—

*Tumor doses in colorectal cancer are significantly lower ($p < 0.05$) with anti-CEA antibodies than with Mu-9.

†Tumor/red marrow and tumor/whole-body ratios of colorectal and medullary thyroid cancer patients are significantly higher at $p < 0.05$ than in all other tumor types.

‡Tumor doses of medullary thyroid cancers are significantly higher at $p < 0.05$, than in all other cancers.

§The high means and standard deviations of MN-14 in ovarian cancer are due to one patient with exceptionally good targeting and resulting extraordinarily high tumor doses.

RESULTS

Patients, Cancer Types and Pharmacokinetics

Table 1 summarizes the characteristics of the 93 patients with solid, CEA-expressing tumors who underwent RAIT with the ^{131}I-labeled IgG anti-CEA monoclonal antibodies, MN-14, hMN-14 and NP-4, as well as the anti-CSAp Mab, Mu-9. Previous studies have shown identical pharmacokinetics of the anti-CEA antibodies NP-4, MN-14, as well as its humanized form, hMN-14, within the same histogenetic tumor type (*12,19*). In contrast, profound differences were found between tumor types, especially between colorectal cancer at elevated plasma CEA levels and other CEA-expressing tumor types (*12*). This holds true for this patient population as well and, therefore, Table 1 does not further differentiate the different MAbs within the same cancer type.

As was demonstrated in detail in previous studies (*12*), colorectal cancer patients had, at comparable plasma CEA levels, the unique feature of clearing anti-CEA antibodies faster from the blood and whole body than patients with all other CEA-expressing tumors, a phenomenon that we could show to be most likely due to CEA-receptor-mediated clearance of immune complexes between the injected antibody and circulating antigen (*12*). This phenomenon can be seen in the patients included in this study as well (Table 1), whereas the anti-CSAp antibody, Mu-9, shows normal clearance rates in these patients (*12*). Therefore, with anti-CEA antibodies, the blood-$t_{1/2}$s, red marrow and whole-body doses in colorectal cancer patients were approximately only half as high as in patients with all other forms of CEA-expressing tumors ($p < 0.001$). As was shown also in previous studies, tumor targeting and sensitivity were independent of the plasma CEA levels or the antibody protein dose applied (*12*).

Overall Tumor Dosimetry

Table 2 summarizes the overall tumor dosimetry of murine and humanized MN-14, NP-4 and Mu-9, as well as the tumor-to-nontumor ratios observed in HAMA- and HAHA-negative patients. In 119 tumors, no significant overall differences were observed between the various antibodies with respect to absolute tumor doses achieved, as well as tumor-to-normal organ ratios.

Table 3 differentiates these data further according to different histogenetic cancer types. In colorectal cancer patients, tumor doses (cGy/mCi) of the anti-CEA antibodies were significantly lower (about half the value) than with the anti-CSAp antibody, Mu-9 ($p < 0.05$). Interestingly, no significant differences are noticeable between NP-4 and MN-14/hMN-14, despite the tenfold higher affinity of the latter. With Mu-9, the normal organ doses also were higher in colorectal cancer patients, which is a consequence of its lower blood and whole-body clearance as compared to the anti-CEA MAbs. This explains why no differences in the tumor-to-nontumor ratios were found between the four antibodies.

Medullary thyroid cancer patients had the highest tumor doses (two- to threefold higher than all other cancer types), as well as tumor-to-nontumor ratios. Also, no significant difference was observed between MN-14 and NP-4. Although, in other cancer types, absolute tumor doses were comparable to those of colorectal cancer patients, tumor-to-normal organ ratios generally were significantly ($p < 0.05$) lower. This is due

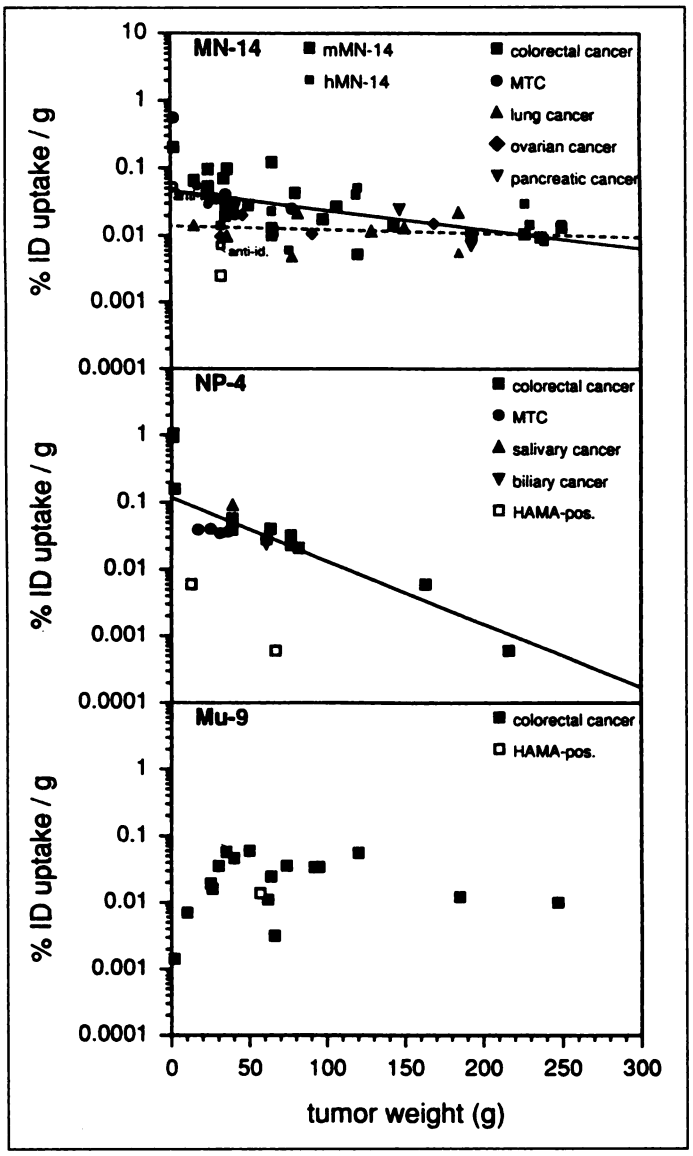

FIGURE 1. Relationship between tumor mass and tumor uptake (expressed as percent of the injected dose per gram) of the anti-CEA antibodies, MN-14 and NP-4, and the anti-CSAp MAb, Mu-9.

to the differences in antibody clearance, leading to higher red marrow and organ doses in these noncolorectal cancer patients.

Quantitative Tumor Uptake in Relationship to Tumor Mass and Cancer Type

Figure 1 shows the relationship between tumor mass and tumor uptake for the three antibodies and different tumor types. The solid line in the upper panel represents the linear regression line for colorectal and medullary thyroid cancer, the dashed one for all other cancer types (difference statistically significant at $p = 0.022$). Open symbols represent data from HAMA-negative (>1000 ng/ml) and HAHA-positive (measured in a complexation assay as described in Methods) patients, respectively. With both anti-CEA antibodies, NP-4 and MN-14, as well as with the MN-14 humanized form, an inverse logarithmic relationship was found when analyzing the overall data of all tumor types (slope statistically significantly different from zero at $p < 0.0001$ for MN-14/hMN-14 [$r = -0.81$], and $p < 0.001$ for NP-4 [$r = -0.91$]). Usually, uptake values ranged between 5×10^{-3} and 10^{-1}%ID/g. Occasionally, in very small tumors (<2 g), uptake values of up to more than 1% of the injected dose per gram were observed, which is higher than would have

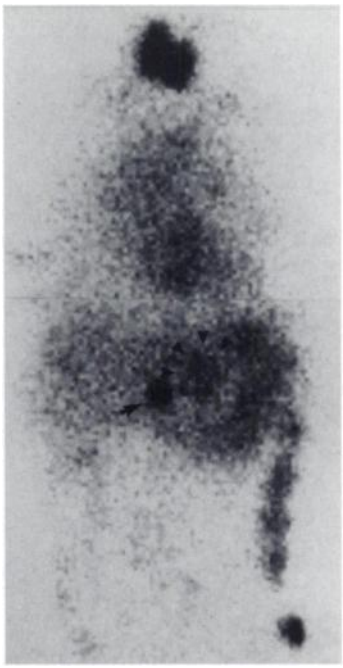

FIGURE 2. Patient 892, a 54-yr-old man with two liver metastases from colorectal cancer (1 and 3 cm diameter). The whole-body scan 120 hr (anterior view) after the injection of ^{131}I-NP-4 IgG shows intense uptake in the small lesion (0.95%ID/g, arrow) and only very moderate uptake (0.05% ID/g) in the larger one (arrowheads).

been predicted by a logarithmic back-extrapolation from the data of larger tumors.

Figure 2 shows, as a typical example, a 54-yr-old patient with two liver metastases from a colorectal cancer (1 and 3 cm in diameter). The scan 120 hr after the injection of ^{131}I-NP-4 IgG showed intense uptake in the small lesion (0.95%ID/g), and only very moderate uptake (0.05%ID/g) in the larger one. Consistently, the smaller lesion responded to RAIT (two injections with 116 mCi/7.8 mg and 159 mCi/8.8 mg ^{131}I-NP-4 IgG 2 mo apart, yielding a calculated total dose of more than 50,000 cGy). This small lesion could not be demonstrated any longer in the 3-mo follow-up CT, whereas the larger one remained essentially unchanged in size.

There was no significant difference in tumor uptake between both anti-CEA antibodies, NP-4 and MN-14, in tumors smaller than 100 g, despite their tenfold difference in affinity (Fig. 1). In larger tumors, the uptake values may be slightly higher for the higher-affinity MN-14 when compared to NP-4. This was statistically significant (slope of the regression line for MN-14 and NP-4 statistically different at $p < 0.001$), but would need to be confirmed by more observations for NP-4.

When differentiating further into different cancer types, at

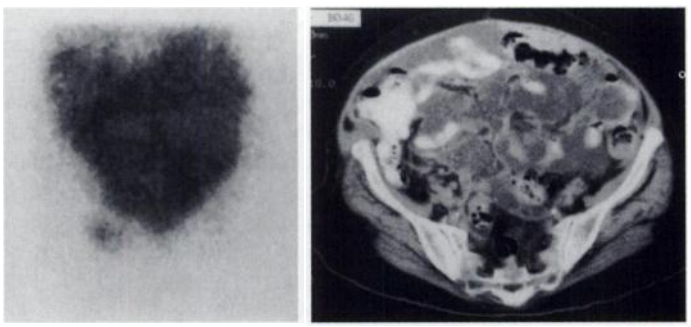

FIGURE 3. Patient 1528, a 72-yr-old woman with diffuse peritoneal carcinomatosis of an ovarian cancer. The scan, performed 72 hr after injection of MN-14 ^{131}I-IgG, shows very strong uptake in the carcinomatosis (ascites).

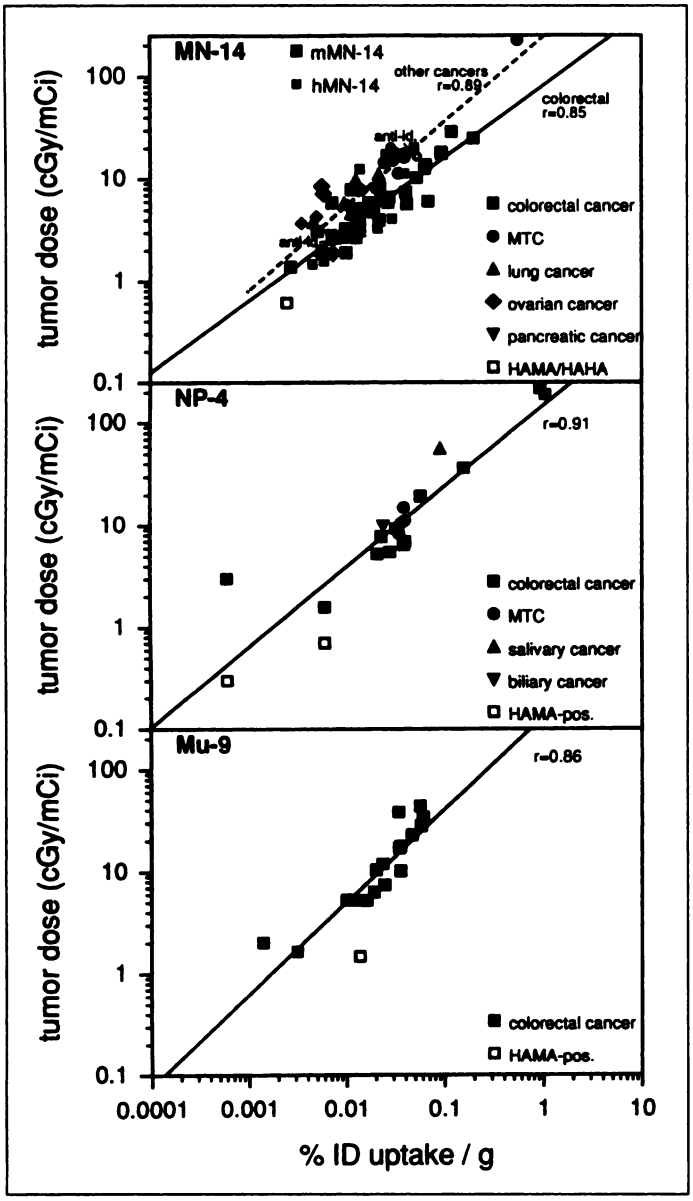

FIGURE 4. Correlation between antibody uptake and the radiation doses.

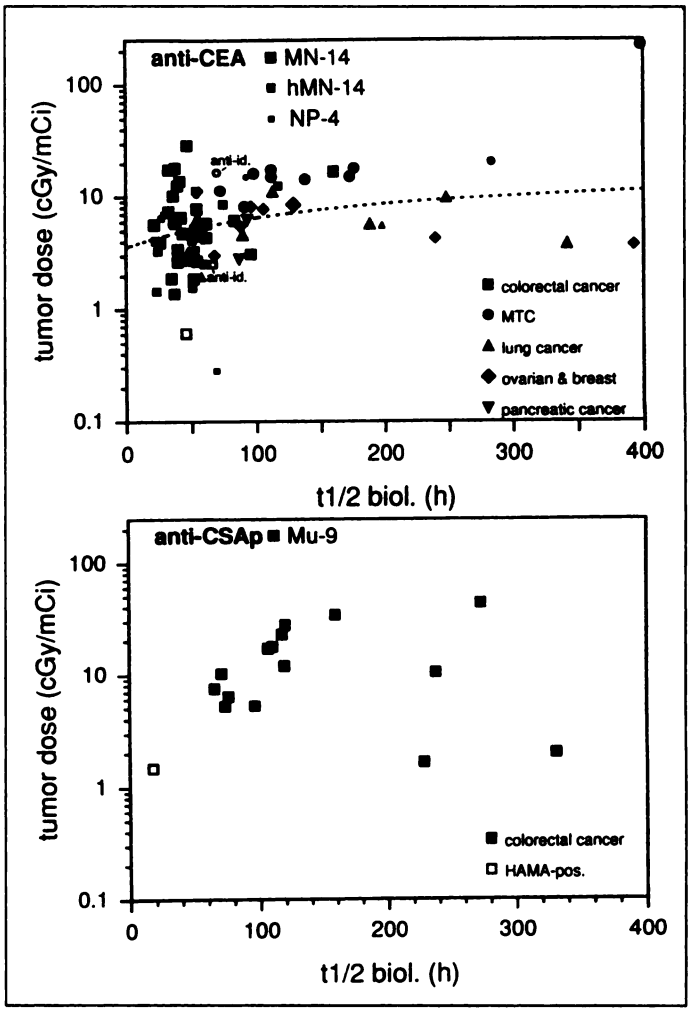

FIGURE 5. Relationship between the biological half-life of the radiolabeled antibody and the tumor doses of anti-CEA and anti-CSAp MAbs.

comparable tumor sizes, the percent tumor uptake values of MN-14 were similar for colorectal and medullary thyroid cancer (overall 0.045% ± 0.075% versus 0.033% ± 0.010% ID/g for colorectal compared with MTC in the size range between 10 and 100 g; solid line in Fig. 1, upper panel). In contrast, the uptake values were significantly lower (0.011% ± 0.007% ID/g) for most other types of CEA-expressing tumors (i.e., lung, pancreatic, etc.) at comparable sizes (dashed line in Fig. 1, upper panel; the difference between the two regression lines [$r = -0.83$ for the solid, $r = -0.71$ for the dashed line] is statistically significant at a $p = 0.022$ level).

However, these macrodosimetric considerations apply only bulky, solid tumors and not to micrometastatic disease. For example, in ovarian cancer, the actual doses to single tumor cells or cell clusters within an ascites may be much higher than estimated from an imaging-based macrodosimetry. Figure 3 shows, as an example, a 72-yr-old woman with diffuse peritoneal carcinomatosis of an ovarian cancer. The scan 72 hr after the injection of MN-14 ^{131}I-IgG shows very high uptake in the carcinomatosis (ascites). The macrodosimetrically (imaging-based) calculated dose was 8.5 cGy/mCi, but the actual microdosimetry to single tumor cells or cell clusters within the ascites may be much higher than estimated from an imaging-based macrodosimetry. This is consistent with an antitumor response (complete remission) achieved in this patient.

No tendency towards higher tumor uptake in smaller tumors was seen with the anti-CSAp antibody, Mu-9 (i.e., the slope of a regression line between tumor size and uptake is not significantly different from zero). Indeed, small tumors even tended toward lower uptake values than were observed in larger ones (Fig. 1, lower panel).

Determinants of Tumor Dosimetry

Figure 4 shows the relationship between tumor uptake and tumor doses achieved. A strong linear relationship was found for all three antibodies between the logarithm of tumor uptake and the logarithm of the radiation doses achieved to the tumors ($r = 0.85$–0.91, slope highly significantly different from zero; $p < 0.0001$). Interestingly, with MN-14 and its humanized form, at comparable absolute uptake values, all noncolorectal-cancer lesions resulted in higher tumor doses than colorectal cancer lesions (Fig. 4, top; dashed compared with solid regression line; difference between both lines significant at $p = 0.0232$). There may be an identical trend with NP-4 (Fig. 4, middle panel), but the difference is only subtle, and the number of observations is too few to reach statistical significance.

Since a radiation dose to a given tissue is defined by the uptake and the effective half-life of the radioisotope in this tissue, this phenomenon must rely on differences in the biological half-lives of the radiolabeled antibody in the tumor. Indeed,

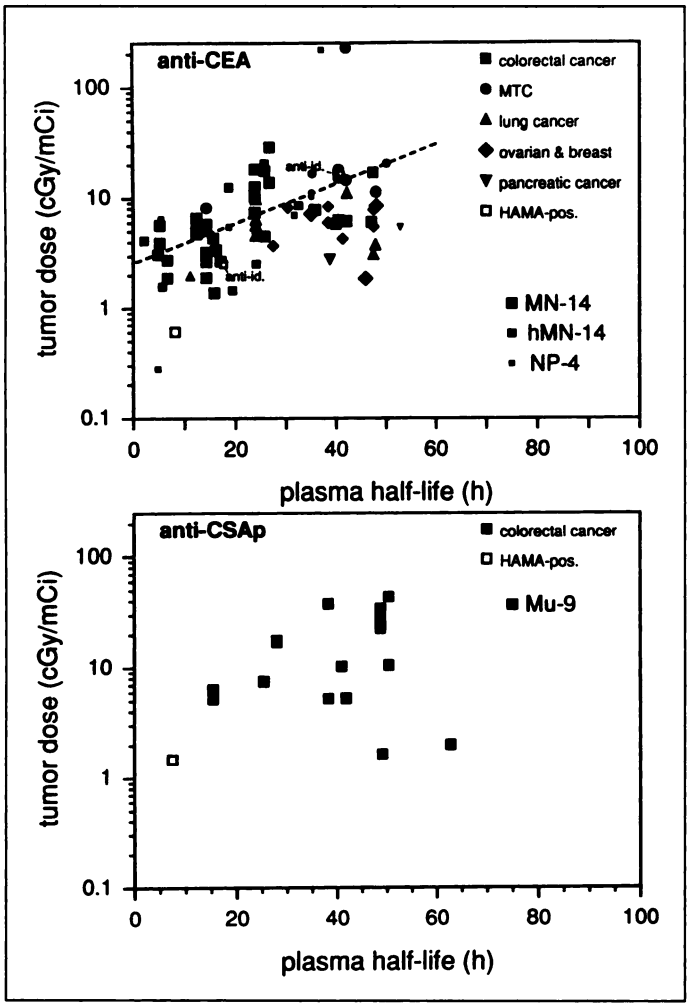

FIGURE 6. Relationship between the plasma-$t_{1/2}$ of the radiolabeled antibody and tumor dosimetry with anti-CEA (upper panel) and anti-CSAp MAbs (lower panel).

Figure 5 shows that the biological half-lives of the anti-CEA antibodies in colorectal tumors were significantly shorter (48.6 hr ± 19.8 hr) than in all other types of cancer (132.9 hr ± 68.8 hr; $p < 0.01$). The higher tumor doses in medullary thyroid cancer at comparable tumor sizes are, therefore, a consequence of a higher tumor uptake (which is similar to colorectal cancer, see above), and of a longer biological $t_{1/2}$ than in colorectal cancer, resulting in a longer residence time in the tumor. In contrast to the strong correlation between uptake values and doses, however, the overall correlation between tumor half-lives and doses was, at $r = 0.51$, rather weak (Fig. 5). The dashed line in Figure 5 represents the regression line between the biological $t_{1/2}$s and the logarithm of the tumor doses ($r = 0.51$; slope significantly different from zero at $p = 0.03$). The regression curve was obtained by computing the linear correlation between the effective $t_{1/2}$s and doses. The equation describing this line was transformed by substituting the effective $t_{1/2}$ by the biological $t_{1/2}$ according to $t_{1/2\ biol} = (1/t_{1/2\ eff} - 1/t_{1/2\ phys})^{-1}$.

A trend was noticed towards shorter tumor half-lives with NP-4 as compared to MN-14. In most cancer types, biological tumor half-lives of NP-4 were approximately half the values obtained with MN-14. Due to a relatively broad variation and the small number of observations, however, statistical significance was reached only in colorectal (33.7 hr ± 10.6 hr versus 52.6 hr ± 23.5 hr for NP-4 and MN-14; $p < 0.05$) and medullary thyroid cancer (61.4 hr ± 21.3 hr versus 124.6 hr ± 36.7 hr for NP-4 and MN-14, respectively; $p < 0.01$).

Since we assumed that the shorter tumor half-lives in colorectal cancer are most likely due to their shorter blood and whole-body half-lives, the relationship between the plasma-$t_{1/2}$ and the tumor doses also was examined (Fig. 6). For colorectal cancers, increasing tumor doses and tumor-to-nontumor ratios were found with increasing half-lives in blood (the dashed line in the upper panel of Fig. 6 represents the linear regression line between the blood-$t_{1/2}$ and the logarithm of the tumor doses in colorectal cancer patients), whereas in all other tumor types the tumor dosimetry was independent of the the plasma $t_{1/2}$s.

Influence of HAMA and HAHA on Tumor Dosimetry

The absolute tumor uptake, as well as the resulting radiation doses, were by 1 to 2 orders of magnitude lower in patients with pre-existing HAMA at the time of antibody injection, depending on the actual HAMA titer (Figs. 1, 4–6; all patients shown with HAMA in these graphs had levels above 1000 ng/ml at the time of their antibody injection). Also, tumor-to-red marrow and tumor-to-other normal organ ratios were significantly lower in these patients than in HAMA-negative patients (data not

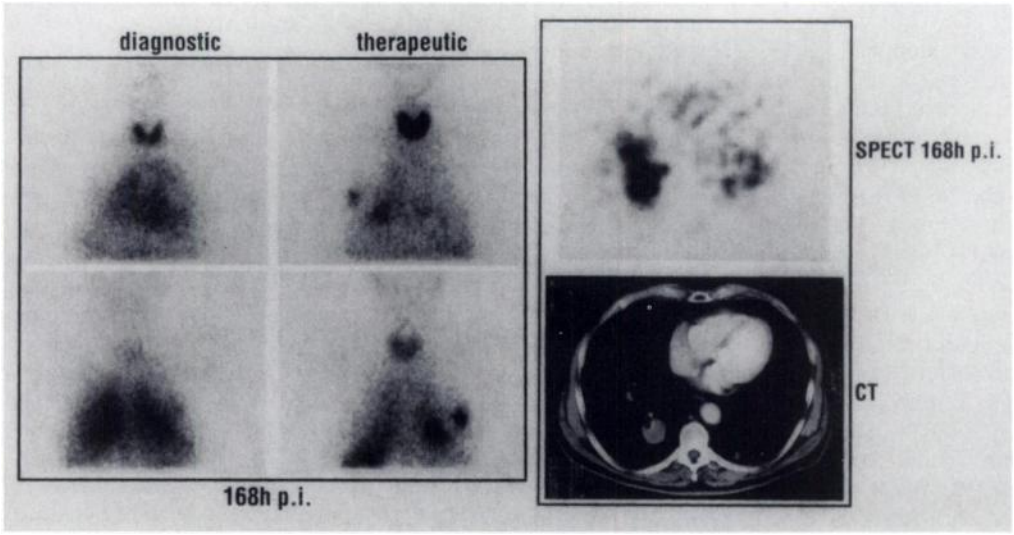

FIGURE 7. Patient 1615, a 62-yr-old man with lung metastases of a rectal cancer (plasma CEA 2.3 ng/ml) developed HAMA under therapy but remained HAMA-negative for at least the first 72 hr after the therapy injection (kinetics in Fig. 8, right panel). SPECT at 168 hr postinjection (therapy injection), in comparison to the CT, shows high MAb retention in the tumor, whereas the blood pool (heart, lungs) is almost completely cleared.

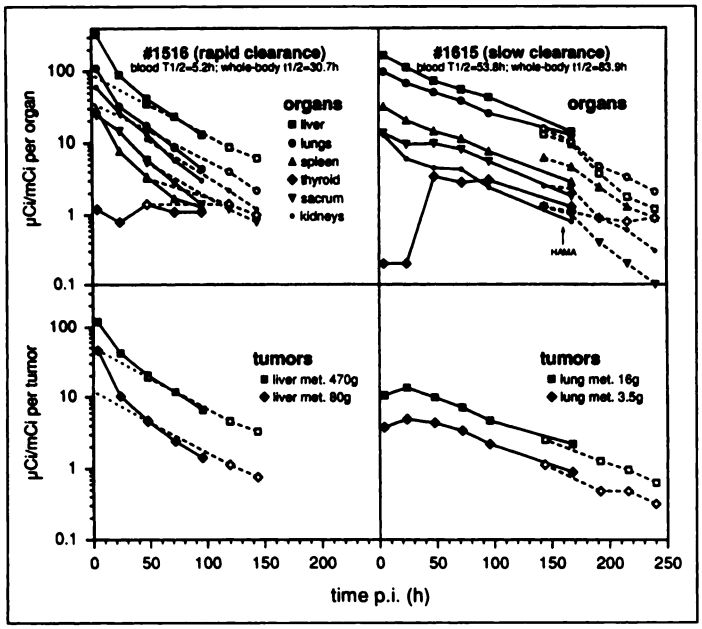

FIGURE 8. MAb targeting kinetics. Solid symbols and lines show the diagnostic, open symbols and dashed lines the respective therapeutic injection. HAMA development in Patient 1615 during therapy (starting approximately 150 hr postinjection) led to an enhanced organ clearance without significantly affecting tumor kinetics.

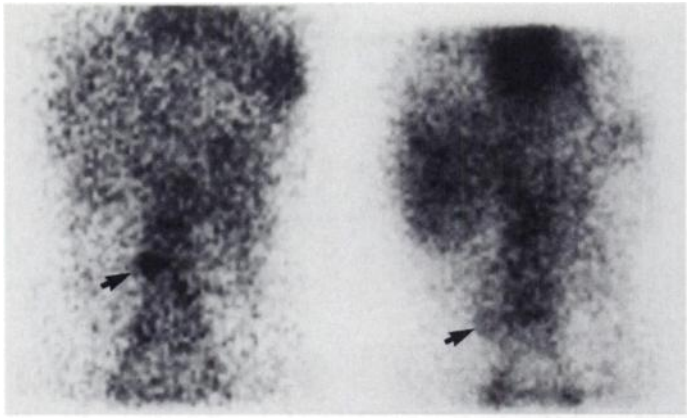

FIGURE 9. Patient 1517, a 31-yr-old man with colorectal cancer and pre-exposure to B72.3. The left scan made with hMN-14 shows strong accumulation in a peritoneal implant (arrow), as well as delineation of the whole peritoneal cavity (peritoneal carcinomatosis). After the development of HAMA to murine MN-14, including anti-idiotypic HAHA, a second diagnostic study with hMN-14 3 mo later (right scan) showed only faint targeting despite no significant alterations in the overall pharmacokinetics.

shown). An exception to this rule was when HAMA developed several days after antibody administration, when tumor targeting had already reached its apogee. In this situation, tumor targeting was not compromised, and the HAMA-induced enhanced background clearance led to markedly enhanced tumor-to-nontumor ratios. An example is Patient 1615, a 62-yr-old man with lung metastases of a rectal cancer (plasma CEA 2.3 ng/ml) who was HAMA-negative in his diagnostic study but developed HAMA during therapy, approximately 7 days after the radioantibody injection (Fig. 7; for kinetics, Fig. 8, right panel). The comparison of diagnostic and therapeutic imaging at 168 hr postinjection (Fig. 7) shows much better tumor-to-background ratios in therapy due to a HAMA-induced enhanced background clearance. Tumor uptake (14.3 versus 17.1 and 7.5 versus 8.7 $\times$ 10^{-2} %ID/g in the 3.5-g and 16-g lesions, respectively, for the therapeutic compared with diagnostic injection) was not influenced; the biological tumor half-lives (97 hr versus 107 hr and 67 hr versus 93 hr) were only slightly affected by this late developing HAMA. The resulting tumor doses were not compromised at 65.3 and 33.7 cGy/mCi.

Whereas HAMA hindered tumor accretion because of rapid uptake of the injected antibody by the reticuloendothelial system of the liver, spleen and bone marrow, with rapid metabolism and excretion of the metabolites through the urine (Behr et al., unpublished data), the influence of human antihumanized MN-14 (HAHA) on tumor uptake was different in patients with anti-idiotypic HAHA against the antigen-binding site of MN-14. Figure 9 shows Patient 1517, a 31-yr-old man with a history of poorly-differentiated metastatic colorectal cancer after chronic ulcerative colitis. His first exposure to murine IgG was an ^{111}In-labeled B72.3 study 8 mo before the first MN-14 IgG scan. At this time-point he was HAMA- and HAHA-negative. The scan with hMN-14 (0.6 mg, 8.1 mCi ^{131}I) shows strong accumulation in a peritoneal implant (tumor uptake 15 $\times$ 10^{-3} %ID/g in a 30-g lesion), as well as delineation of the whole peritoneal cavity (peritoneal carcinomatosis). One week after receiving 6.0 mg of murine MN-14 IgG for RAIT, he developed HAMA, including an anti-idiotypic response (HAHA). A second diagnostic study with 10.0 mg hMN-14 3 mo later showed only faint targeting (uptake only approximately 7 $\times$ 10^{-3} %ID/g in the 30-g implant, in other words less than half of the original value), and absence of targeting of the peritoneal carcinomatosis, despite there being no significant alterations in the overall pharmakokinetics (blood-$t_{1/2}$ 17.65 hr compared with 18.63 hr in the first study 3 mo earlier).

Tumor Targeting Kinetics

Different targeting kinetics were seen between the antibodies in patients with different tumor types. With MN-14, the maximal tumor uptake was seen in 10 of 28 assessable patients by 4 hr (all of them had plasma $t_{1/2}$ shorter than 15 hr), in 12 patients by 24 hr, and in five patients at 48 hr postinjection. Consistent with the short blood half-life of anti-CEA antibodies in this cancer type, in 8 of 14 colorectal cancer patients, the maximum uptake was reached already at 4 hr, whereas in four assessable lung cancer patients, two had maximal tumor uptake at 48 hr, and one even at 72 hr postinjection. In accordance with the longer serum half-lives of Mu-9 in colorectal cancer patients, maximal tumor uptake was seen in two of seven assessable patients at 24 hr, and in the other five of seven patients at 48 hr postinjection.

With anti-CEA antibodies in the group of colorectal cancer patients, the time of maximal tumor uptake depended on how fast the antibody cleared from blood. Figure 8 shows two typical organ and tumor targeting profiles for a rapidly, as well as a normally clearing colorectal cancer patient. In patients with plasma half-lives longer than 30 hr, usually a monoexponential clearance pattern from the normal organs and the whole-body was observed (Fig. 8, right panel). In this situation, tumor targeting was seen over 24 to 48 hr postinjection. In contrast, colorectal cancer patients with rapid clearance followed a biexponential organ and whole-body clearance pattern (Fig. 8, left panel), tumor uptake being confined to only the first few hours. In contrast, plasma-CEA level-matched colorectal cancer patients showed a monoexponential clearance pattern with the anti-CSAp Mab, Mu-9.

DISCUSSION

Whereas in lymphoma, probably due to its radiosensitivity, complete response rates of over 80% have been reported with RAIT (*1,2*), the objective response rates are still rather low in

solid tumors (*2,3*, and Behr et al., unpublished data). In external beam radiation, doses between 30 and 70 Gy are required for achieving responses in adenocarcinomas. Although some recent studies showed higher or at least a comparable effectiveness of low dose-rate RAIT (*26*), the generally accepted view is that even higher radiation doses are necessary to achieve a similar biological effectiveness, especially given the lower dose rate of RAIT. Our study, therefore, has attempted to identify subgroups of patients which may be especially suitable for a radioimmunotherapeutic approach. Several preclinical studies have attempted to define the relationship between tumor size, antigen expression, interstitial pressure, vascular leakage, etc., and tumor uptake with radiolabeled antibodies (*8–11*). Also, mathematical models were developed to describe these data (*7,9*). However, only a few studies exist that examine these parameters in patients.

An inverse relationship between tumor size (mass) and absolute tumor uptake of antibody is a well-known phenomenon (*8–10,28–30*). In these small lesions, probably optimal conditions are found with respect to vascularization, antigen accessibilty, interstitial pressure, and several other factors (*7–11*). No such relationship exists with Mu-9, which recognizes a mucin found intracellularly, as well as in especially high concentrations in necrotic tumor tissue (*20*), which is more abundant in larger tumors. This may explain why small lesions had an even lower Mu-9 uptake than larger ones. Interesting is the fact that with the anti-CEA antibodies, extraordinarily high uptake values have been observed in very small lesions, resulting in tumor doses exceeding 100 cGy/mCi. This favors the concept of radioimmunotherapy as a treatment modality for either minimal residual disease or in adjuvant settings (*5*).

The observation that a tenfold difference in affinity does not lead to any significant difference in tumor uptake was observed in clinical studies by others as well (*31,32*), which is in contrast to data from animal (*16,17*) or mathematical models (*33*). Our data indicate, however, that the difference in affinity might cause a different retention of antibody in the tumor. Longer half-lives in the tumor are consistent with the superior imaging qualities of MN-14, when compared to NP-4 (*17*). Earlier studies on the uptake of antibodies of different affinity were usually relying on well counter measurements of tumor biopsy specimens. This method may have advantages with respect to the accuracy of the absolute uptake determination, but this single time-point sampling does not allow the determination of the biological tumor $t_{1/2}$ (*31,32*). This is probably the reason why such differences in tumor half-lives with antibodies of different affinity have not been described until now.

In contrast to reported data on $Na^{131}I$ therapy of differentiated thyroid cancer, where the retention-half-life of the nuclide in the tumor was identified as the major dose-determining value (*27*), in radioimmunotherapy the absolute antibody uptake is the most important factor determining the actual tumor dose. The shorter tumor half-lives in colorectal cancer patients, when compared to other cancer types, are most likely due to their shorter blood half-lives. In a recent study (*12*), we showed that colorectal cancer patients have a tendency to clear anti-CEA antibodies quickly from the circulation (most likely a CEA-receptor-mediated clearance of immune complexes between CEA and the MAb). In contrast, Mu-9 showed a normal pharmacokinetic behavior in these patients (*12*), since its mucin epitope is not recognized in the circulation (*20*). These different clearance rates are most likely due to microheterogeneities in the chemical structure of the CEA produced by different cancer types (*12,34,35*).

The highest tumor uptake values of MAb were observed for colorectal and medullary thyroid cancer patients. Due to their longer half-lives, the latter had higher mean doses when compared to most colorectal tumors. Taking into account the general hypervascularity (*15,36*) as compared to hypovascular colorectal tumors, our study suggests that CEA antigen content is highest in colorectal and medullary thyroid cancer. Uptake in all other cancer types was found to be significantly lower, suggesting a lower CEA content, which would be in accordance with the lower CEA plasma levels generally observed in patients with these other cancer types.

Due to the short blood half-life, the uptake is confined to only some hours in colorectal cancer patients with rapid clearance, with the consequence of lower tumor doses. In those patients with larger lesions, Mu-9, as an antimucin antibody, may clearly have a therapeutic advantage over CEA Mabs.

Therapeutic tumor dosimetry is based on imaging data that were obtained several days after the antibody injection, relying on a (monoexponential) back-extrapolation to earlier time points. This suggests that the therapeutic dosimetry underestimates the actual tumor doses in rapidly-clearing situations (dotted lines in Fig. 8, left panel); the back-extrapolation will yield an accurate dose estimate only in slow-clearing patients with monoexponentially-defined clearance rates, whereas the dotted lines in Figure 8 (left panel) show that in the biexponential clearance situation, pseudolinear back-extrapolation from the imaging data at later time points would lead to a substantial underestimation of the actual doses. Thus, any analysis of the predictability of the therapeutic from the diagnostic tumor dosimetry must be interpreted with great caution (*12*), and it was, therefore, not performed in this study.

It is a well-known fact that HAMA leads to rapid blood and whole-body clearance with subsequently decreased tumor uptakes and doses (*22*). It is interesting in this context that late-developing HAMA (after maximum tumor uptake has occurred) does not compromise tumor targeting, but enhances the later tumor-to-nontumor ratios (Figs. 7 and 8). This observation favors the further development of second-antibody clearing strategies (*37*). Anti-idiotypic responses, in contrast to conventional HAMA, do not seem to affect the overall biodistribution, but compromise the tumor targeting ability of the circulating antibody, most likely by blocking its antigen-binding site. This fundamental difference between classical HAMA and anti-idiotypic HAHA has recently been predicted from animal data by Pimm (*38*).

Our study suggests that especially favorable tumor doses can be achieved in small lesions of colorectal cancer, as well as in medullary thyroid cancer, although comparably favorable conditions also may be found in other neoplasms with micrometastatic lesions. The predicted tumor doses may exceed by far the values generally obtainable with external beam radiation. Therefore, an adjuvant RAIT trial or a therapy of minimal disease in these tumor types seems to be warranted (*39,40*).

ACKNOWLEDGMENTS

We thank M. Przyblowski, D. Varga and L. Ince for preparations and quality assurance of the labeled antibodies, I. Magill and B. Magrys for assistance in immunoassays and processing pharmacokinetic data, D. Dunlop for imaging and dosimetry assistance, R. Vagg for data management and V. Reddick and K. Diccianni for patient follow-up. These studies were supported in part by grants from the Deutsche Forschungsgemeinschaft (DFG Be 1689/1-1/2) and the National Institutes of Health (CA39841 and CA54425). This work is dedicated to Professor F. Wolf, MD, University of Erlangen-Nuremberg, Erlangen, Germany, on the occasion of his 65th birthday

REFERENCES

1. Press OW, Eary JF, Appelbaum FR, et al. Phase II trial of ^{131}I-B1 (anti-CD20) antibody therapy with autologous stem cell transplantation for relapsed B cell lymphoma. *Lancet* 1995;346:336–340.
2. Goldenberg DM, ed. *Cancer therapy with radiolabeled antibodies*. Boca Raton, FL; CRC Press; 1995.
3. Divgi CR, Scott AM, Dantis L, et al. Phase I radioimmunotherapy trial with iodine-131-CC49 in metastatic colon carcinoma. *J Nucl Med* 1995;36:586–592.
4. Blumenthal RD, Sharkey RM, Natale AM, et al. Comparison of equitoxic radioimmunotherapy and chemotherapy in the treatment of human colonic cancer xenografts. *Cancer Res* 1994;54:142–151.
5. Blumenthal RD, Sharkey RM, Haywood L, et al. Targeted therapy of athymic mice bearing GW-39 human colonic cancer micrometastases with ^{131}I-labeled monoclonal antibodies. *Cancer Res* 1992;52:6036–6044.
6. Mach JP, Carrel S, Merenda C, Heumann D, Roenspies U. In vivo localization of anti-CEA antibody in colon carcinoma. Can results obtained in the nude mice model be extrapolated to the patient situation? *Eur J Cancer* 1978;(suppl I):113–120.
7. Jain RK. Determination of tumor blood flow: a review. *Cancer Res* 1988;48: 2641–2658.
8. Hagan PL, Halpern SE, Dillman RO, et al. Tumor size: effect on monoclonal antibody uptake in tumor nodules. *J Nucl Med* 1986;27:422–427.
9. Williams LE, Duda RB, Proffitt RT, et al. Tumor uptake as a function of tumor mass: a mathematical model. *J Nucl Med* 1988;29:103–109.
10. Boerman OC, Sharkey RM, Blumenthal RD, Aninipot RL, Goldenberg DM. The presence of a concomitant bulky tumor can decrease the uptake and therapeutic efficacy of radiolabeled antibodies in small tumors. *Int J Cancer* 1992;51:470–475.
11. Juweid M, Neumann R, Paik C, et al. Micropharmacology of monoclonal antibodies in solid tumors: direct experimental evidence for a binding site barrier. *Cancer Res* 1992;52:5144–5153.
12. Behr TM, Sharkey RM, Juweid ME, et al. Factors influencing the pharmacokinetics, dosimetry and diagnostic accuracy of radioimmunodetection and radioimmunotherapy of CEA-expressing tumors. *Cancer Res* 1996;56:1805–1816.
13. Behr TM, Sharkey RM, Juweid ME, et al. Phase I/II clinical radioimmunotherapy with an ^{131}I-labeled anti-CEA murine monoclonal antibody IgG. *J Nucl Med* 1997:in press.
14. Juweid ME, Sharkey RM, Behr TM, et al. Pilot studies of radioimmunotherapy in patients with CEA-producing cancers and small-volume disease using ^{131}I-NP-4 F(ab')$_2$ anti-CEA monoclonal antibody. *J Nucl Med* 1996;37:1504–1510.
15. Juweid ME, Sharkey RM, Behr T, et al. Radioimmunotherapy of medullary thyroid carcinoma with ^{131}I-labeled anti-CEA antibodies: Initial results. *J Nucl Med* 1996;37 (in press).
16. Sharkey RM, Goldenberg DM, Goldenberg H, et al. Murine monoclonal antibodies against carcinoembryonic antigen: immunological, pharmacokinetic, and targeting properties in humans. *Cancer Res* 1990;50:2823–2831.
17. Sharkey RM, Goldenberg DM, Murthy S, et al. Clinical evaluation of tumor targeting with a high-affinity, anticarcinoembryonic-antigen-specific, murine monoclonal antibody, MN-14. *Cancer* 1993;71:2082–2096.
18. Primus FJ, Newell KD, Blue A, Goldenberg DM. Immunological heterogeneity of carcinoembryonic antigen: antigenic determinants on carcinoembryonic antigen distinguished by monoclonal antibodies. *Cancer Res* 1983;43:686–692.
19. Sharkey RM, Juweid M, Shevitz J, et al. Evaluation of a CDR-grafted (humanized) anti-carcinoembryonic antigen (CEA) monoclonal antibody in preclinical and clinical studies. *Cancer Res* 1995;55:5935s-5945s.
20. Sharkey RM, Goldenberg DM, Vagg R, et al. Phase I clinical evaluation of a new murine monoclonal antibody (Mu-9) against colon-specific antigen-p for targeting gastrointestinal carcinomas. *Cancer* 1994;73:864–877.
21. Wu RK, Siegel JA. Absolute quantitation of radioactivity using the buildup factor. *Med Phys* 1984;11:189–192.
22. Siegel JA, Pawlyk DA, Lee RE, et al. Tumor, red marrow, and organ dosimetry for ^{131}I-labeled anti-carcinoembryonic antigen monoclonal antibody. *Cancer Res* 1990; 50:1039s-1042s.
23. Pawlyk DA, Siegel JA, Sharkey RM, Goldenberg DM. Automating large-scale processing of dosimetry data [Abstract]. *J Nucl Med* 1993;34(suppl):160P.
24. Dunn RM, Juweid ME, Behr TM, Siegel JA, Sharkey RM, Goldenberg DM. An automated internal dosimetry scheme for radiolabeled antibodies. *Med Phys* 1995;22: 1549–1550.
25. Becker RA, Chambers JM, Wilks AR. *The new S language: a program environment for data analysis and graphics*. Pacific Grove, CA: Wadsworth and Brooks; 1988.
26. Buchsbaum D, Khazaeli MB, Liu T, et al. Fractionated radioimmunotherapy of human colon carcinoma xenografts with ^{131}I-labeled monoclonal antibody CC49. *Cancer Res* 1995;55:5881s-5887s.
27. Maxon HR, Thomas SR, Hertzberg VS, et al. Relation between effective radiation dose and outcome of radioiodine therapy for thyroid cancer. *N Engl J Med* 1983;309:937–941.
28. Murray JL, Mujoo K, Wilmanns C, Mansfield P, Wilbur DS, Rosenblum MG. Variables influencing tumor uptake of anti-melanoma monoclonal antibodies radioiodinated using para-iodobenzoyl (PIB) conjugate. *J Nucl Med* 1991;32:279–287.
29. Philben VJ, Jakowatz JG, Beatty BG, et al. The effect of tumor CEA content and tumor size in tissue uptake of indium-111-labeled anti-CEA monoclonal antibody. *Cancer* 1986;57:571–576.
30. Watanabe Y, Endo K, Koizumi M, et al. Effect of tumor mass and antigenic nature on the biodistribution of labeled monoclonal antibodies in mice. *Cancer Res* 1989;49: 2884–2889.
31. Gallinger S, Reilly RM, Kirsh JC, et al. Comparative dual label study of first and second generation antitumor-associated glycoprotein-72 monoclonal antibodies in colorectal cancer patients. *Cancer Res* 1993;53:271–278.
32. Divgi CR, Scott AM, McDermott K, et al. Clinical comparison of radiolocalization of two monoclonal antibodies (mAbs) against the TAG-72 antigen. *Nucl Med Biol* 1994;21:9–15.
33. Thomas GD, Chappell MJ, Dykes PW, et al. Effect of dose, molecular size, affinity, and protein binding on tumor uptake of antibody or ligand: a biomathematical model. *Cancer Res* 1989;49:3290–3296.
34. Hernando JJ, von Kleist S, Grunert F. A repertoire of monoclonal antibodies reveals extensive epitope heterogeneity in CEA purified from neoplasms originating from different organs. *Int J Cancer* 1994;56:655–661.
35. Thomas P, Toth CA, Saini KS, Jessup JM, Steele G. The structure, metabolism and function of the carcinoembryonic antigen gene family. *Biochim Biophys Acta* 1990; 1032:177–189.
36. Bressler EL, Alpern MB, Glazer GM, Francis IR, Ensminger WD. Hypervascular hepatic metastases. *Radiology* 1987;162:49–51.
37. Goldenberg DM, Sharkey RM, Ford E. Anti-antibody enhancement of iodine-131 anti-CEA radioimmunodetection in experimental and clinical studies. *J Nucl Med* 1987;28:1604–1610.
38. Pimm MV. Possible consequences of human antibody responses on the biodistribution of fragments of human, humanized or chimeric monoclonal antibodies: a note of caution. *Life Sci* 1994;55:45–49.
39. Sgouros G. Radioimmunotherapy of micrometastases: side-stepping the solid-tumor hurdle [Editorial]. *J Nucl Med* 1995;36:1910–1912.
40. Dunn RM, Juweid ME, Behr TM, Siegel JA, Sharkey RM, Goldenberg DM. Dosimetric potential of minimal residual disease using radiolabeled antibodies [Abstract]. *J Nucl Med* 1996;37(suppl):44P.